Highly Efficient Motion-Corrected Simultaneous Cardiac PET-MR Imaging

Camila Munoz, Radhouene Neji, Paul Marsden, Andrew J. Reader, René M. Botnar and Claudia Prieto

***Abstract*—MR-based motion correction of PET data has been proposed as a high-impact application for improving image quality and myocardial tissue quantification in cardiac PET-MR imaging. However, current PET-MR motion compensation schemes acquire only motion information from MR data during PET acquisition time and diagnostic MR images afterwards, significantly increasing total exam time. Here we propose an efficient acquisition and reconstruction scheme for simultaneous cardiac PET-MR imaging that acquires both diagnostic and motion information from MR, with motion information being used to correct both PET and MR data. The proposed MR acquisition scheme includes acquiring low-resolution 2D image navigators at each heartbeat by spatially encoding the start-up echoes of an ECG-gated gradient echo sequence, allowing for 100% MR scan efficiency (i.e. all data is accepted for reconstruction, reducing scan time). These 2D image navigators are then used to estimate foot-head and right-left motion of the heart during the respiratory cycle in a beat-to-beat fashion, providing motion estimates to translationally correct and bin the MR data. MR images from each respiratory bin are used to estimate 3D non-rigid motion between respiratory bins. These non-rigid motion fields are then used for correcting both the MR and PET data. Results from healthy volunteers show that motion correction improves MR visualisation of the right and left anterior descending coronary arteries. A simulated PET acquisition showed improvements in contrast of the myocardium and better depiction of papillary muscles when applying motion correction. The presented framework improves image quality and contrast compared with uncorrected images for both MR and PET images.**

I. Introduction

The recent development of simultaneous PET-MR scanners has broadened the possibilities for comprehensive non-invasive assessment of cardiovascular disease in a single examination [1]. This could be achieved by using complementary information between the modalities, e.g. for quantification of myocardial perfusion and assessment of coronary artery stenosis. However, image degradation due to physiological motion during data acquisition in both modalities remains a major challenge.

Current cardiac PET-MR research concentrates mainly on improving the quality of PET images using MR information [2]. These approaches propose acquiring simultaneous MR images as motion surrogates for MR-based PET motion correction, using sequences that are not usually part of the diagnostic MR protocol. This leads to long acquisition times since diagnostic MR images need to be acquired after the simultaneous PET-MR acquisition.

Here we propose an acquisition and reconstruction framework for acquiring coronary MR angiography (CMRA) and cardiac PET in a single examination. Motion is estimated from MR images, so that 2D translational and 3D non-rigid motion corrected CMRA can be performed on a PET-MR system, while simultaneously providing non-rigid motion fields for MR-based PET respiratory motion correction. This approach is highly efficient since all acquired MR data is used for reconstruction (100% scan efficiency), resulting in shorter scan time than conventional 1D navigator gated MR acquisitions.

II. Materials and Methods

A. MR Acquisition and Reconstruction

An ECG-triggered 3D T1-weighted spoiled gradient echo sequence using a fully sampled golden-step Cartesian spiral profile order [3] was implemented. This trajectory samples the phase encoding plane following approximate spiral interleaves on the Cartesian grid. A low-resolution 2D image navigator (iNav) is acquired at each heartbeat before the CMRA acquisition (Fig. 1), by spatially encoding low flip angle start-up echoes of the acquisition [4].

Reconstruction of the MR data is performed in two steps (Fig. 2). In the first step, translational motion in foot-head (FH) and right-left (RL) directions is estimated from the iNavs in a beat-to-beat fashion using cross correlation of a template covering the apex of the heart (Fig. 2a). These motion estimates are used to correct CMRA data acquired at each heartbeat prior to image reconstruction.

In a second step, the estimated FH motion is used to bin the CMRA data in translationally motion corrected respiratory

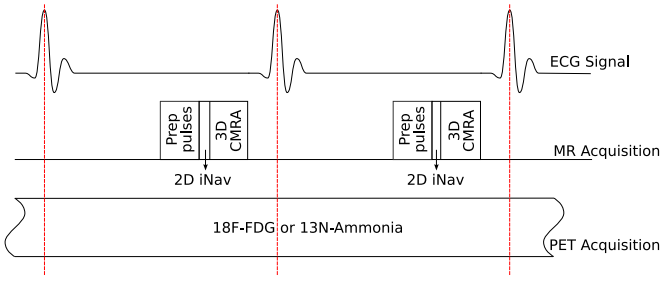

Fig. 1. Acquisition scheme. Diagnostic CMRA is acquired simultaneously with cardiac PET data.

C. Munoz, R. Neji, P. Marsden, A.J. Reader, R.M. Botnar, and C.Prieto are with the Department of Biomedical Engineering, Division of Imaging Sciences and Biomedical Engineering, King's College London, UK.

R. Neji is with MR Research Collaborations, Siemens Healthcare, Frimley, UK.

This work was funded by the King's College London & Imperial College London EPSRC Centre for Doctoral Training in Medical Imaging (Grant number: EP/L015226/1).

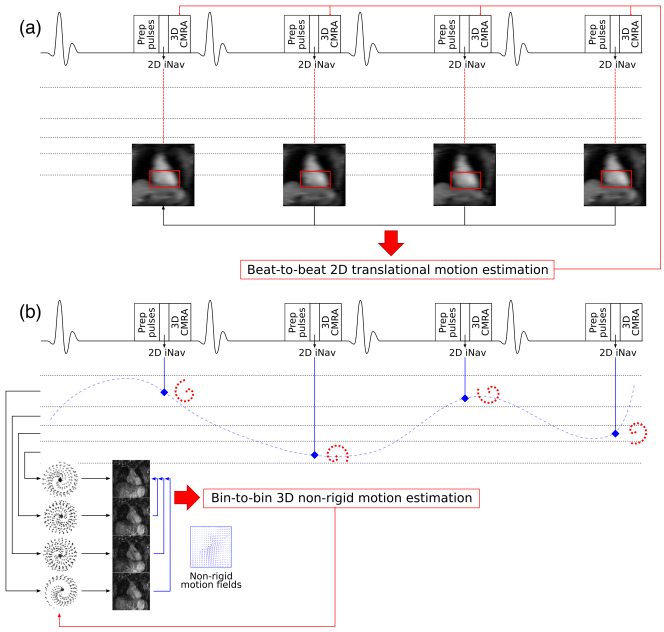

Fig. 2. (a) Beat-to-beat and (b) bin-to-bin motion estimation and correction scheme for MR. FH and RL motion are estimated from low-resolution 2D image navigators and used to translationally correct the CMRA data. FH motion is then used to bin the CMRA data. 3D non-rigid motion is estimated from images reconstructed at each respiratory bin and used in a motion corrected reconstruction framework.

bins. Reconstructed images at each respiratory position are then used to estimate 3D non-rigid motion in a bin-to-bin fashion (Fig. 2b), using the end-expiration bin as reference. The 3D non-rigid motion fields are finally incorporated in a General Matrix Description (GMD) reconstruction framework [3], [5].

B. PET Reconstruction

PET data is binned using the estimated FH motion from MR, so that the motion information obtained from MR is used to correct PET data in a bin-to-bin fashion. Using a motion compensated image reconstruction (MCIR) approach, non-rigid motion is included in the system matrix by modifying both the emission and attenuation maps, as shown in Equation 1 [6].

$$\boldsymbol{\rho}^{(s+1)} = \frac{\boldsymbol{\rho}^{(s)}}{\sum_k (\mathbf{M}^k)^T \mathbf{P}^T \mathbf{N} \mathbf{A}^k \mathbf{1}_I} \times \sum_k (\mathbf{M}^k)^T \mathbf{P}^T \frac{{\mathbf{s_{tot}}}^k}{\mathbf{P}\mathbf{M}^k \boldsymbol{\rho}^{(s)} + (\mathbf{N}\mathbf{A}^k)^{-1}\mathbf{b}} \quad (1)$$

where $\boldsymbol{\rho}^{(s)}$ is a column vector that contains the PET voxel values at iteration s in the reference bin (i.e. end-expiration), $\mathbf{M}^k$ is the motion operator estimated from MR that transforms an image at reference bin to a bin k, $\mathbf{P}$ is a matrix that models the system forward-projection, $\mathbf{N}$ is the normalisation matrix, $\mathbf{A}^k$ is a matrix containing attenuation correction factors for bin k, ${\mathbf{s_{tot}}}^k$ is a column vector containing the counts detected in bin k and $\mathbf{b}$ represents an estimation of background (i.e. scatter and random) coincidences. This approach assumes that background coincidences vary slowly compared to the emission map, so the effect of motion on them is neglected.

C. Experiments

Three healthy subjects were scanned during free-breathing on a 3T PET-MR scanner (Biograph mMR, Siemens Healthcare, Erlangen, Germany) using a prototype implementation of the proposed MR sequence (field of view = $300 \times 300 \times 80\text{mm}^3$, resolution = $1 \times 1 \times 2\text{mm}^3$, repetition time/echo time = 3.75/1.72ms, flip angle = $15°$, acquisition window = 90ms). A trigger delay was set targeting the mid-diastolic rest period. For the 2D iNav acquisition, 14 start-up echoes (same field of view, flip angle = $3°$) were used. MR data was reconstructed with (a) the proposed approach, (b) 2D translational motion correction only and (c) without motion correction, for comparison purposes.

An MR-based PET simulation was performed using semi-automatically segmented MR images from one of the volunteers [7]. 3D Dixon MR images were segmented into liver, lungs, myocardium, blood pool, soft tissue and background signal, and realistic attenuation and standardized uptake values (SUV) for 18F-FDG were assigned to the different tissues [8]. The emission and attenuation maps were combined with the motion estimates obtained from MR to simulate respiratory motion. Analytical PET simulations were performed in STIR [9] using the geometry of the scanner, and randoms and scatters were neglected.

PET image reconstruction was performed using the proposed reconstruction method, with 21 subsets, 3 iterations, a voxel size of $2.03 \times 2.08 \times 2.08\text{mm}^3$, a matrix size of $127 \times 285 \times 285$ and a 4mm isotropic Gaussian post-filtering. Additionally, a motion-free image was simulated and reconstructed for reference purposes, and an uncorrected reconstruction was performed for further comparison.

III. Results and Discussion

3D coronary MRA images were reformatted to simultaneously visualise the left anterior descending (LAD) and right coronary artery (RCA). A significant improvement in recovering the distal segment of the RCA (red arrow) and the proximal segment of the LAD (blue arrow) can be observed in Fig. 3, when applying translational motion correction. However, lack of contrast prevented observation of the distal LAD. When applying non-rigid motion correction, the distal LAD can be recovered (green arrow), and the arteries are better depicted.

PET image quality degrades when no motion correction is performed, as can be observed in Fig. 4. Small features such as the papillary muscles are blurred, producing errors in the images (blue arrow). Similarly, thin structures, such as the left atrial myocardium (red arrow) can not be observed in the uncorrected reconstruction. When including motion in the reconstruction, both problems are solved, and contrast between tissues is improved. For a region of interest covering the whole heart a % root-mean-square error of 11.59% and 5.67% were obtained with the uncorrected and motion corrected reconstructions, respectively, compared to the motion free reference.

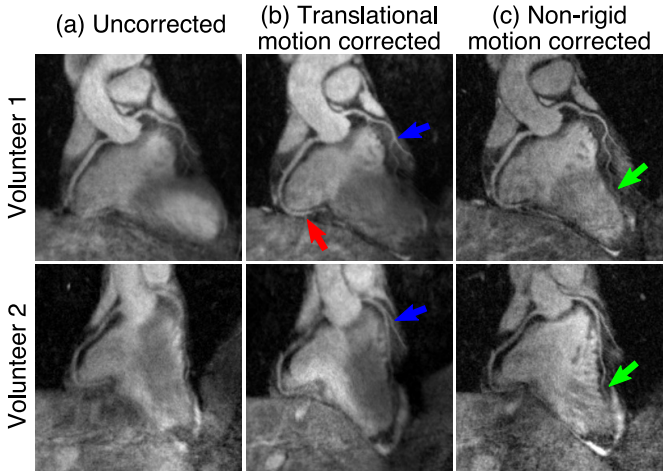

Fig. 3. Reformatted images along the RCA and LAD artery from two healthy subjects. (a) Uncorrected images, (b) translational and (c) non-rigid motion corrected images. The proximal RCA (red arrow) and the proximal LAD (blue arrow) can be observed in (b), but non-rigid motion correction (c) is required to recover the distal LAD (green arrow).

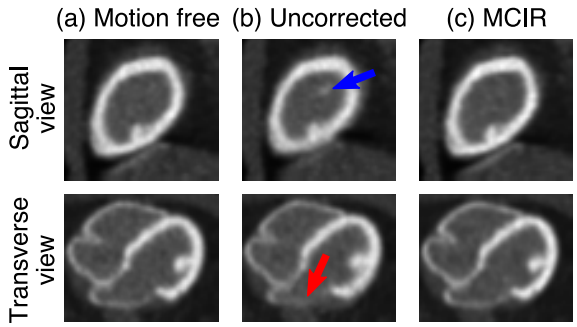

Fig. 4. Example sagittal and transverse planes from reconstructed PET images. (a) Motion free reference, (b) uncorrected and (c) motion corrected images. If no motion correction is performed, artefacts due to blurring (blue arrow) occur and thin structures (red arrow) can not be observed. Both problems are solved when using MR-based motion corrected image reconstruction.

IV. Conclusion

This study presents a framework that allows for 2D translational and 3D non-rigid motion correction of 3D CMRA on a 3T PET-MR scanner, achieving 100% MR scan efficiency while simultaneously providing non-rigid motion fields for MR-based PET motion correction.

The presented motion correction scheme improves image quality and contrast compared with uncorrected images for both MR and PET images. Further validation of PET motion correction in patient data will be performed in future studies.

References

[1] C. Rischpler, S. G. Nekolla, I. Dregely, and M. Schwaiger, "Hybrid PET/MR imaging of the heart: potential, initial experiences, and future prospects." *JNM*, vol. 54, no. 3, pp. 402–15, Mar 2013.

[2] C. Munoz, C. Kolbitsch, A. J. Reader, P. Marsden, T. Schaeffter, and C. Prieto, "MR-Based Cardiac and Respiratory Motion-Compensation Techniques for PET-MR Imaging," *PET Clinics*, vol. 11, no. 2, pp. 179–191, Jan 2016.

[3] C. Prieto, M. Doneva, M. Usman, M. Henningsson, G. Greil, T. Schaeffter, and R. M. Botnar, "Highly efficient respiratory motion compensated free-breathing coronary MRA using golden-step Cartesian acquisition." *JMRI*, vol. 41, no. 3, pp. 738–46, Mar 2015.

[4] M. Henningsson, P. Koken, C. Stehning, R. Razavi, C. Prieto, and R. M. Botnar, "Whole-heart coronary MR angiography with 2D self-navigated image reconstruction." *MRM*, vol. 67, no. 2, pp. 437–45, Feb 2012.

[5] P. G. Batchelor, D. Atkinson, P. Irarrazaval, D. L. G. Hill, J. Hajnal, and D. Larkman, "Matrix description of general motion correction applied to multishot images." *MRM*, vol. 54, no. 5, pp. 1273–80, Nov 2005.

[6] Y. Petibon, G. El Fakhri, R. Nezafat, N. Johnson, T. J. Brady, and J. Ouyang, "Towards coronary plaque imaging using simultaneous PET-MR: a simulation study." *PMB*, vol. 59, no. 5, pp. 1203–22, Mar 2014.

[7] C. Tsoumpas, C. Buerger, A. P. King, P. Mollet, V. Keereman, S. Vandenberghe, V. Schulz, P. J. Schleyer, T. Schaeffter, and P. K. Marsden, "Fast generation of 4D PET-MR data from real dynamic MR acquisitions." *PMB*, vol. 56, no. 20, pp. 6597–613, Oct 2011.

[8] Y. Wang, E. Chiu, J. Rosenberg, and S. S. Gambhir, "Standardized uptake value atlas: Characterization of physiological 2-Deoxy-2-[18F]fluoro-d-glucose uptake in normal tissues," *Molecular Imaging and Biology*, vol. 9, no. 2, pp. 83–90, 2007.

[9] K. Thielemans, C. Tsoumpas, S. Mustafovic, T. Beisel, P. Aguiar, N. Dikaios, and M. W. Jacobson, "STIR: software for tomographic image reconstruction release 2," *PMB*, vol. 57, no. 4, pp. 867–883, Feb 2012.